An efficient 3D magnetotelluric data inversion scheme for large models

Arun Singh, Department of Applied Geophysics, Indian Institute of Technology (ISM), Dhanbad*
Rahul Dehiya, Department of Earth and Climate Science, IISER, Pune

*arunsingh2626@gmail.com

Keywords

3D Magnetotelluric Inversion, Radiation Boundary Method, USArray

Abstract

In this study, we present a 3D magnetotelluric inversion scheme based on the concept of the radiation boundary method. In this scheme, the forward modeling and gradient computations are done in two steps. The key advantage of the proposed scheme is its ability to handle arbitrarily shaped inversion domains, defined based on the distribution of the sites, thus reducing the number of unknown model parameters that are not constrained by the data. Additionally, the two-step computation process significantly improves the accuracy and efficiency of the solutions as compared to the traditional inversion algorithm. The efficiency of the developed algorithm is tested over different synthetic data sets generated for various geological scenarios and over the USArray MT Transportable Array project, a continental scale dataset. The final inverted resistivity model for USArray data set is similar to the models reported previously but with fine resolution.

Introduction

The Magnetotelluric (MT) techniques belong to the class of geophysical methods that help to delineate the subsurface conductivity distribution. In the MT method, time-varying orthogonal components of electric (two horizontal) and magnetic fields (two horizontal and one vertical) are recorded. From the recorded dataset, transfer functions such as impedance and tipper data are derived at selected frequencies. Using the dataset, the subsurface conductivity distribution is obtained through inversion. Several 3D inversion algorithms have been developed such as 3DINV (Avdeev & Avdeeva, 2009a), ModEM (Egbert & Kelbert, 2012), AP3DMT (Singh et al., 2017), and others. However, even with the advanced computational facilities and efficient algorithms, the 3D MT data inversion is still computationally very intensive. The problem may become computationally intractable for very large models (large number of unknown model parameters). Such large models arise due to fine resolution or large aerial extent of the survey area. To reduce the computation time one generally works with a subset of the dataset or a coarse mesh or decimated dataset spatially covering the survey area.
To address the problem of inversion for large models, we propose a new inversion approach based on the Radiation Boundary (RB) method. The developed scheme is very efficient as compared to the traditional inversion approach. The concept of RB has been used previously to improve the efficiency of 3D forward modeling for controlled-source electromagnetic (Dehiya, 2021) and the MT method (Singh & Dehiya, 2023). In this approach, two meshes are required, a coarse and fine mesh with the desired resolution. The coarse mesh is similar to the mesh that is typically used in inversion whereas the fine mesh is the central part of the coarse mesh but without any padded grids (except a few grids in air) and the desired resolution. Also, the fine mesh can have arbitrary shapes depending on the location of the MT sites. The developed scheme is tested over the USArray data set (Schultz et al., 2006-2018) and is used to produce a high-resolution resistivity model.

Method

Inverse modeling aims to find a model **m** while fitting the observed data within the given error bounds by minimizing a pre-defined penalty function. The penalty function is defined as a sum of weighted data misfit and model regularization. The contribution of these two is balanced using a real scalar known as the regularization parameter. The minimization of the penalty function is iterative in nature i.e., one starts with an initial guess model and the model is updated at each iteration till the final

model is obtained. The optimization techniques such as Gauss-Newton (Constable et al., 1987; Siripunvaraporn et al., 2005a) quasi-newton (Avdeev & Avdeeva, 2009b) Non-linear conjugate gradient (Rodi & Mackie, 2001; Newman & Boggs, 2004; Kelbert et al., 2014) are the preferred ones for inversion algorithms. In all these schemes, the computations of forward responses and the product of the Jacobian (sensitivity) matrix with a vector are required.

For the proposed scheme, we have made modifications to AP3DMT, a MATLAB-based code for 3D MT inversion (Singh et al., 2017). In this code, the staggered grid finite difference (FD) is used for computing the forward responses. The use of the FD scheme leads to a sparse system written as

$$\mathbf{Ae} = \mathbf{s} \quad (1)$$

where **A** is the complex, sparse system matrix, **e** is the nodal electric field and **s** is the boundary condition vector. The system is solved using an iterative solver resulting in an efficient and low-memory task. For efficient computation, the Jacobian, **J** for the source frequency, f is expressed as the product of three matrices as

$$\mathbf{J} = \mathbf{LA}^{-1}\mathbf{P} \quad (2)$$

where **P**, denotes the product of the coefficient matrix derivative with respect to the model parameter and electric field; $\mathbf{A}^{-1}$ is the inverse of the system matrix and **L** maps the derivative of the EM solution to the derivative of the predicted data. For details one can refer to Egbert and Kelbert (2012); Singh et al. (2017)

In the traditional algorithms, the same mesh is used for modeling and inversion. The mesh has two parts, a core central part and an extended (padded) part to enforce necessary boundary conditions. The central part has the desired resolution and in the extended part, grid spacing increases rapidly (generally on a log scale) in order to use few grids while discretizing a large space. Due to the extended part, the condition number of the system increases resulting in a slow convergence of the iterative solver.

To alleviate the issue, we employ a two-step numerical simulation using two meshes. The coarse mesh is a traditional mesh but with coarse resolution in the central part and the fine mesh has only the core central part with the desired resolution and no padded grids except very few grids in the air. The gradient is computed using these two meshes as shown in Figure 1. The model parameters, corresponding to the fine mesh are updated after each iteration hence a mapping is required to update the model parameters on the coarse mesh. We have used the volume average of the log conductivity of cells that lie within the volume of the coarse grid cell. Since, this approach allows arbitrary choice of the boundary surface for the fine mesh (see Figure 1) where the boundary condition vector, $\mathbf{e}_f$, can be calculated.

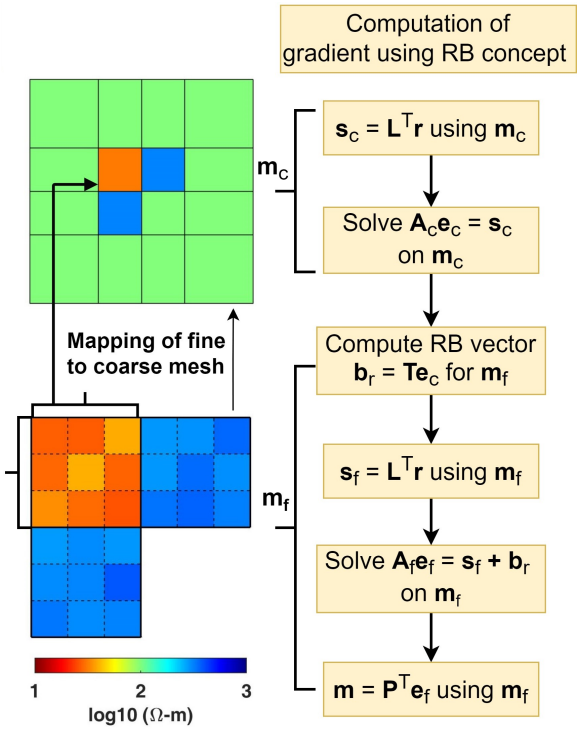

Figure 1: Flowchart showing the computation of forward response and product of transpose of Jacobian with a residual vector (data space vector) using the coarse and fine meshes defined as $\mathbf{m}_c$ and $\mathbf{m}_f$ respectively

USArray Data Inversion

Long-period MT (~10–20,000 s) sites on a quasi-regular 70 km grid, covering much of the continental United States (US) have been collected through the EarthScope, USArray MT Transportable Array project. A total of 1116 sites were recorded from 2006-2018 and the MT transfer functions (full impedance and Tipper) are archived. Based on the quality of the data, each site is rated from 1 to 5, 5 being the site with the highest quality (Imamura &

Schultz, 2020). Previously subsets of the dataset have been inverted (e.g., Patro & Egbert, 2008; Meqbel et al., 2014). Recently Yang et al., 2021 presented a 3D continental-scale electrical resistivity model. The authors used only 423 sites with at least a rating of 3. The inter-site spacing is approximately 120 km. The authors kept the horizontal resolution at 30 km in order to model the possible galvanic distortion and to keep the problem computationally tractable.

To make the data set, we chose all the sites with data quality from 1 to 5. A few sites and bad data points were removed based on the visual inspection of the data. To mitigate the influence of external sources on Tipper data, we have considered periods less than 3000s (Egbert, 1989). Thus the final data set has 1007 sites (see Figure 2 for the location of the sites) with impedance at 30 periods and Tipper at 25 periods. The error floor is set a 5% of the product of off-diagonal components of the impedance tensor for all the elements of the impedance tensor and 0.03 for the Tipper. If the site rating is 3 or less then the error floor becomes 10% and 0.05 respectively.

For the RB scheme, the coarse mesh was set at 65x117x57 (excluding 12 layers in the air) and the central part has a resolution of 60 km. We added a total of 44 grid layers in both horizontal directions as padding. The thickness of the initial layer was set to 50 m and logarithmically increased to 125 km at the lowermost part of the domain. The fine mesh has a resolution of 15x20 km. The grids in the z-direction are similar to the coarse model but with reduced depth. With such discretization, the mesh size becomes 160x261x52 (excluding 6 layers in air). The ocean bathymetry was taken from the ETOPO1 global topographic data set, and seawater with resistivity of 0.3 ohm-m was fixed during the inversion. No topography was considered. A polygon, represented as a black dashed line in Figure 2 was defined and the unknown model parameters outside the polygon were discarded resulting in the reduction of model parameters by ~38%. The selected data set was inverted in two steps.

In the first step, the dataset was inverted using a traditional algorithm with a coarse mesh. From the resulting inverted model, an initial guess model is obtained for the subsequent fine mesh inversion. The normalized root mean square (nRMS) reduces to 2.5 in 132 NLCG iterations. The distribution of site-wise data misfit shows a generally uniform pattern, with higher nRMS values observed along the east coast. Notably, the nRMS values are lower for intermediate periods ranging from 50 to 1000 s, while slightly larger nRMS values are observed for shorter and longer periods. A similar misfit pattern has been previously documented (Yang et al., 2021; Munch & Grayver, 2023).

The horizontal slice view of the final model at different depth planes is shown in Figure 3. The primary lithospheric characteristics in the final model align with geological settings and exhibit similarity to those reported in the previous studies (Meqbel et al., 2014; Yang et al., 2021; Munch & Grayver, 2023). We observe a distinct geological transition from the tectonically active margin in the western region to the

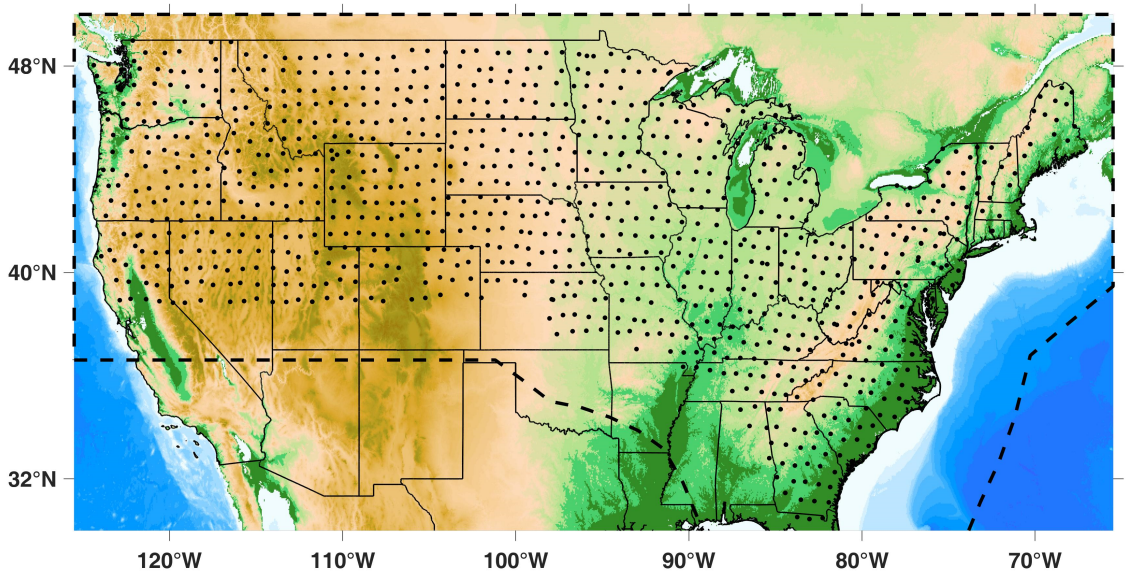

Figure 2: Map of showing the USArray measurement sites considered for the inversion as black dots. For the fine model, model parameters (approximately 38%) outside the black dashed polygon were discarded.

comparatively stable North American Craton in the eastern region. The high conductivity values are primarily associated with the North American Central Plains (NACP) conductors beneath the North Basin and Range area in the west, as well as the Appalachians. On the other hand, the low conductivity values are attributed to the Superior (SC) and Wyoming (WC) cratons, the Medicine Hat Block (MHB), and an east coast parallel resistor located beneath the southeastern US (SEUS).

Conclusion

The 3D MT inversion scheme based on RB method is employed to perform the inversion of the USArray MT dataset. The irregular distribution of MT sites, primarily determined by the geography of the USA, offers flexibility in designing an arbitrary shape for the inversion domain. This advantage allows for efficient reduction in the number of unknown parameters, making the inversion problem computationally tractable while enabling fine resolution. The two-step simulation process of the RB results in more accurate and efficient computations of forward responses as reported previously. The proposed scheme can be implemented in any standard inversion algorithm by making necessary modifications to the subroutines dealing with forward and gradient computations

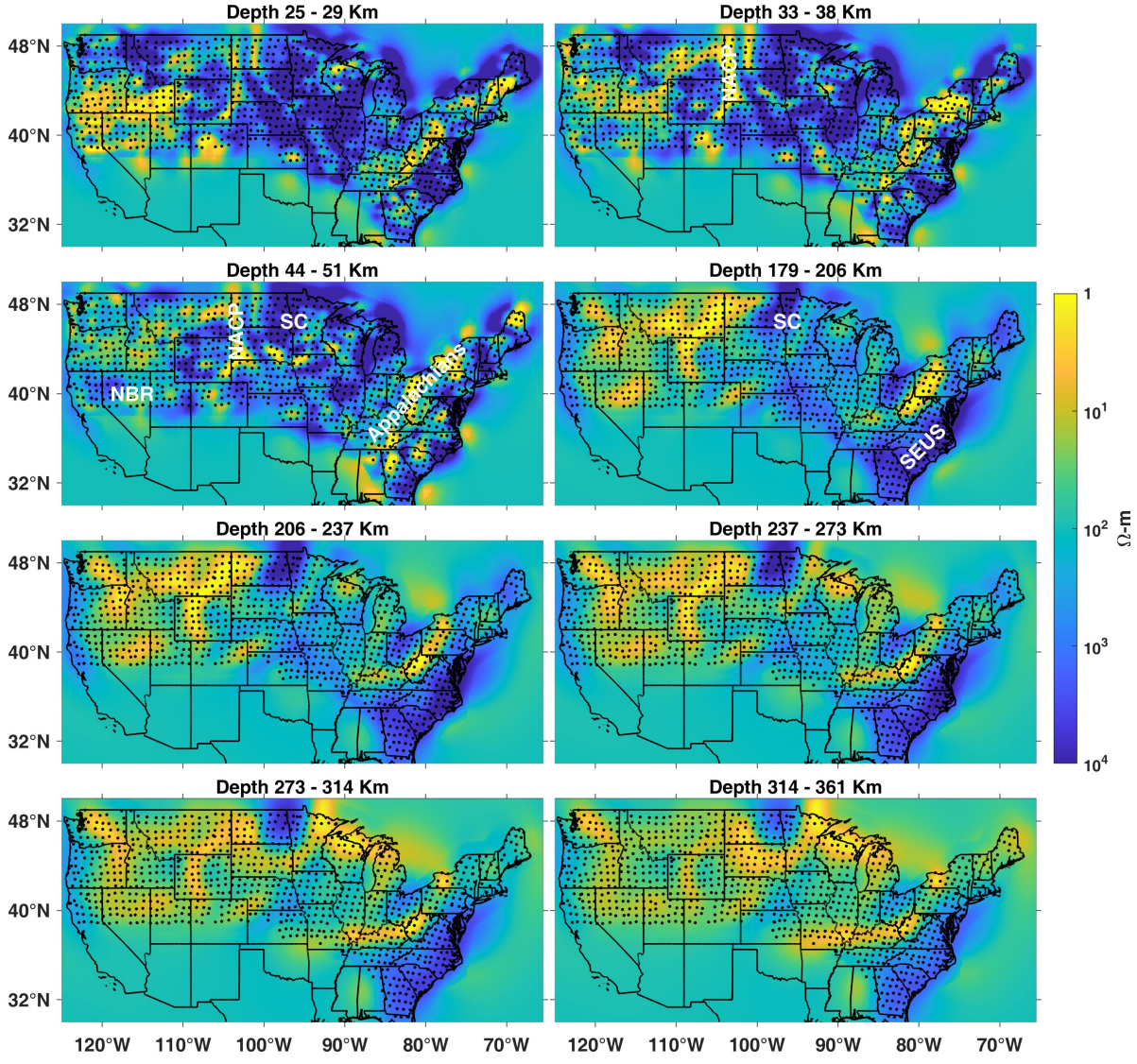

Figure 3: Image showing selected sections for final resistivity model at various depths.

An efficient 3D magnetotelluric data inversion scheme for large models

References

Avdeev, D., and Avdeeva, A., 2009a, 3d magnetotelluric inversion using a limited memory quasi-newton optimization; Geophysics, 74 (3), F45-F57.

Constable, C. S., Parker, R. L., and Constable, C. G., 1987, Occam's inversion: a practical algorithm for generating smooth models from electromagnetic sounding data; Geophysics, 52 , 289–300.

Dehiya, R., 2021, 3d forward modeling of controlled-source electromagnetic data based on the radiation boundary method; Geophysics, 86 (2), E143–E155.

Egbert, G. D., 1989, Multivariate analysis of geomagnetic array data: 2. random source models; Journal of Geophysical Research: Solid Earth, 94 (B10), 14249-14265

Egbert, G. D., and Kelbert, A., 2012, Computational recipes for electromagnetic inverse problems; Geophysical Journal International, 188 , 251–267.

Imamura, N., and Schultz, A., 2020, Quality estimation of magnetotelluric impedance tensors using neural networks; The Leading Edge, 39 (10), 702–710.

Kelbert, A., Meqbel, N., Egbert, G. D., and Tandon, K., 2014, ModEM: a modular system for inversion of electromagnetic geophysical data; Computers and Geosciences, 66 , 40-53.

Meqbel, N., Egbert, G. D., Wannamaker, P. E., Kelbert, A., and Schultz, A., 2014, Deep electrical resistivity structure of the northwestern u.s. derived from 3-d inversion of usarray magnetotelluric data; Earth and Planetary Science Letters, 402 , 290-304.

Munch, F. D., and Grayver, A., 2023, Multi-scale imaging of 3-d electrical conductivity structure under the contiguous us constrains lateral variations in the upper mantle water content; Earth and Planetary Science Letters, 602 , 117939

Newman, G. A., and Boggs, P. T., 2004. Solution accelerators for large-scale three-dimensional electromagnetic inverse problems; Inverse Problem, 20 , S151–S170

Patro, P. K., and Egbert, G. D., 2008; Regional conductivity structure of Cascadia: preliminary results from 3D inversion of USA array transportable array Magnetotelluric data; Geophysical Research Letters, 35, art. no. L20311.678

Rodi, W. L., and Mackie, R. L., 2001; Nonlinear conjugate gradients algorithm for 2D magnetotelluric inversion; Geophysics, 66 , 174–187.

Schultz, A., Egbert, G., Kelbert, A., Peery, T., Clote, V., Fry, B., and Erofeeva, S., 2006-2018, Staff of the national geoelectromagnetic facility and their contractors (2006–2018), usarray TA magnetotelluric transfer functions.

Singh, A., and Dehiya, R., 2023, An efficient em modeling scheme for large 3-d models-a magnetotelluric case study; IEEE Transactions on Geoscience and Remote Sensing, 61, 1-11.

Singh, A., Dehiya, R., Gupta, P. K., and Israil, M., 2017, A MATLAB based 3D modeling and inversion code for MT data; Computers and Geosciences, 14 , 1-11

Siripunvaraporn, W., Egbert, G., Lenbury, Y., and Uyeshima, M., 2005a, Three-dimensional magnetotelluric inversion: data-space method; Physics of the Earth and Planetary Interiors, 150, 3–14.

Yang, B., Egbert, G. D., Zhang, H., Meqbel, N., and Hu, X., 2021, Electrical resistivity imaging of continental united states from three-dimensional inversion of earthscope usarray magnetotelluric data; Earth and Planetary Science Letters,706 , 117244.

Acknowledgments

The computational facilities were generated using the Faculty Research Grant No. FRS (161)/2021-2022/AGP provided to the first author by the host institute. The authors are thankful to the USarray team for making the MT data set available at the IRIS SPUD repository (http://ds.iris.edu/spud/emtf).